J Appl Electrochem (2014) 44:1145–1151
DOI 10.1007/s10800-014-0726-7

RESEARCH ARTICLE

Mini-chunk biochar supercapacitors

Lei Zhang · Junhua Jiang · Nancy Holm · Fangling Chen

Received: 12 May 2014 / Accepted: 28 July 2014 / Published online: 17 August 2014

Abstract Biochar prepared from the pyrolysis of maple wood was studied as supercapacitor electrode materials. Three kinds of electrodes were fabricated: mini-chunk electrodes, thin-film electrodes, and large-disk-chunk electrodes. Their capacitive behaviors were studied using cyclic voltammetry, galvanostatic charge–discharge, and electrochemical impedance spectroscopy. The mini-chunk supercapacitor shows an electrochemical behavior similar to the supercapacitor using the thin-film electrodes. It exhibits outstanding performance characteristic of a high specific capacitance of approximately 32 F g^{-1} and a high stability without obvious capacitance decays upon 2,600 potential cycles. This indicates that the mini-chunk supercapacitor can be used as an mF-scale power source for electronic device applications. Moreover, the mini-chunk electrode provides a simple and fast technique to evaluate biochar materials used as potentially high-performance, low-cost, and environmental friendly supercapacitor electrodes without the need of binder and complicated fabrication procedures. However, the supercapacitor using large-disk-chunk biochar electrodes shows lower specific capacitive performance due to the high ohmic resistance stemming from long tubular structures within biochar.

Keywords Supercapacitor · Biochar · Mini-chunk electrode · Thin-film electrode · Maple wood

L. Zhang (✉) · J. Jiang · N. Holm
Illinois Sustainable Technology Center, University of Illinois at Urbana-Champaign, Champaign, IL 61820, USA
e-mail: leizha@cec.sc.edu

L. Zhang · F. Chen
Department of Mechanical Engineering, University of South Carolina, Columbia, SC 29208, USA

1 Introduction

The need to store and use energy on diverse scales in a modern technological society necessitates the design of large and small energy systems, among which electrical energy storage systems have attracted much interest in the past several decades [1]. Supercapacitors, also known as ultracapacitors or electrochemical double-layer capacitors, are energy storage devices with high power density, fast charge and discharge rate, and long service life [2]. It can complement or replace batteries in electrical energy storage and harvesting applications, when high-rate power delivery or uptake is needed [3–5]. Small-scale supercapacitors can be integrated with microelectronic devices to work as stand-alone power sources or as efficient energy storage units complementing batteries and energy harvesters, leading to wider use of these devices in many industries [6].

Various materials have been investigated as promising electrode materials for supercapacitors and been generally categorized into two major classes: (1) pseudocapacitive materials such as metal hydroxides [7], transition metal oxides [8, 9] and conducting polymers [10]; and (2) carbon-based materials in which charging–discharging follows an electric double-layer mechanism. Carbon materials have been widely used in supercapacitors because of their low cost, versatile existing forms (for example powders, fibers, felts, composites, mats, monoliths, and foils), and easy processability [11]. Because of various forms of carbon materials, designs of the electrodes for supercapacitors are diverse. Thin-film electrodes are the most widely used. They are normally fabricated by mixing carbon materials with binder to make slurry followed by printing or rolling to make film electrodes [12, 13]. In some cases, ready-made carbon materials with flat appearance such as carbon

paper or carbon foil were used as electrodes directly [14, 15].

Biochar is a novel carbon-rich material produced through the pyrolysis of biomass such as wood, shell, husks, or crop residues [16, 17]. The production of biochar is low cost and environmental friendly [18]. A two-step process is usually pursued for the preparation of the electrode materials of biochar supercapacitor: a carbonization of biomass into biochar and a post-activation of the biochar [19]. The carbonation of biomass is often performed with heating temperature range from 500 to 900 °C in a low oxygen atmosphere [18, 20]. The post-activation is achieved by mixing the precursor with an activating reagent such as H_3PO_4, $ZnCl_2$, and KOH, then removing the unreacted chemicals [20–22]. In some previous works of biochar supercapacitors, the activated biochar shows very promising supercapacitor performance [19, 23, 24]. It has been recently reported by our group that ultra-high carbon content biochar can be obtained from red cedar wood and the activation using HNO_3 can effectively increase the number of surface oxygen groups to achieve high capacitance [25].

In the present work, biochar made from maple wood was used as electrodes for supercapacitor in three different forms: mini-chunk, thin-film, and large-disk-chunk. We have found that the biochar supercpacitor using mini-chunk electrodes shows very similar electrochemical behavior and specific capacitance, compared to the supercapacitor using the thin-film electrodes. However, the supercapacitor using the large-disk-chunk electrodes exhibits large ohmic resistance and poor charging and discharging properties. These facts indicate that (1) the mini-chunk biochar supercapacitor can be directly used as an mF-scale supercapacitor power source; and (2) the mini-chunk biochar electrode can provide a simple and fast technique to evaluate various biochar materials for supercapacitor applications.

2 Experimental

2.1 Preparation of biochar

Biochar was prepared through the pyrolysis of maple wood at 750 °C for 2 h in N_2 atmosphere. Pieces of maple chunks were put into quartz tube furnace, with flowing N_2 at 40 mL s^{-1}. The heating treatment was performed at 200 °C for 2 h to remove water content, followed by increasing to 750 °C and held for another 2 h to remove bio-oil and biogas and carbonize biomass into biochar. Both the heating and cooling rate were kept at 3 °C min^{-1}. After the heating treatment, the biochar chunks were made into three types of electrodes for biochar supercapacitors following the procedures described below.

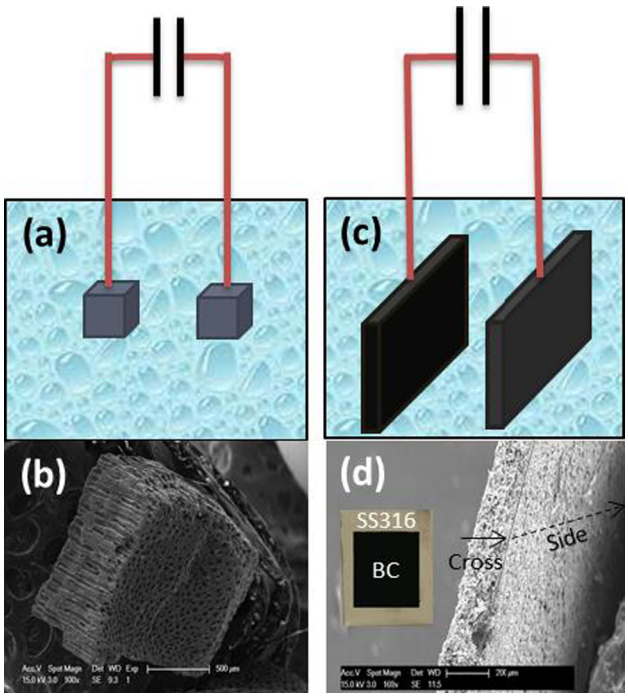

Fig. 1 Schematic diagram of a biochar mini-chunk (**a**) or thin-film (**c**) supercapacitor, and low-resolution SEM images of a biochar mini-chunk (**b**) or thin-film (**d**) electrode. *Insert* to **d** Photo of a 1 × 1 cm^2 biochar thin film supported on a 304 stainless steel shim

2.2 Preparation of supercapacitors

The symmetrical supercapacitors were used for evaluation, and three kinds of designed electrodes were fabricated, including mini-chunk electrodes, thin-film electrodes, and large-disk-chunk electrodes. The mini-chunk electrodes were made from the as-prepared biochar by cutting them into small monoliths of 0.1 cm × 0.1 cm × 0.05 cm and approximately 1.0 mg in mass. Gold wires of 0.01 cm in diameter were used as current collector by wrapping them onto the mini-chunk electrode. The thin-film electrodes were made by printing the slurry made of biochar powder onto stainless steel shims. The preparation procedures were as follows. The carbonized biochar was first ground into powder, from which 0.045 g biochar powder was mixed with 0.10 g 5 wt% Nafion solution. The mixture was ultrasonicated for 10 min to form homogeneous suspension slurry, and then printed onto the stainless steel shims (304 stainless steel with 50 μm in thickness) with an active area of 1 cm × 1 cm. The ink was dried at 120 °C for 2 h in air. After drying, thin films of 200 μm in thickness were formed and adhered onto the stainless steel shims. The large-disk-chunk electrodes were fabricated by cutting the

as-prepared biochar into disk-shaped slices with the geometric area of 0.18 cm^2 and thickness of 700 μm. All electrodes were immersed into 0.5 mol L^{-1} HNO_3 solution at room temperature overnight for the post-activation to increase the surface hydrophilicity and the numbers of surface oxygen groups. The electrodes were rinsed by deionized water before testing. For the capacitive performance evaluation, two similar electrodes were used to construct a supercapacitor and 0.5 mol L^{-1} H_2SO_4 solution was used as electrolyte. The schemes of the supercapacitors with mini-chunk and thin-film electrodes were shown in Fig. 1a, c, respectively.

2.3 Characterization

Morphology of biochar electrodes was characterized using a Philips XL30 ESEM-FEG field-emission environmental scanning electron microscope (SEM) operating at 15 kV. Brunauer–Emmett–Teller (BET) surface area was measured using physical adsorption of nitrogen molecules on the surface of maple biochar powder activated by nitric acid. The BET instrument is a Micromeritics Gemini VII 2390 V1.03 surface area/pore volume analyzer. Raman measurements were performed using a high-resolution research-grade Horiba LabRAM HR 3D-capable Raman spectroscopy imaging system. All electrochemical measurements were conducted using Autolab general purpose electrochemical instrument PGSTAT30 (Metrohm, USA). The capacitive behavior was studied using cyclic voltammograms (CV) recorded at different scan rates and galvanostatic charge–discharge at different current densities. Alternating current (AC) impedance spectra were measured in the frequency range from 1 M to 50 mHz. The stability of a supercapacitor was evaluated by applying potential cycles between −0.5 and 0.5 V to the two symmetrical electrode supercapacitors.

3 Results and discussion

Figure 1b, d are the low-resolution SEM images of the mini-chunk electrodes and thin-film electrodes and Fig. 2 are the magnified SEM images. The mini-chunk electrode in rectangular shape (Fig. 1b) exhibits parallel through chunk channels. Pores with two different sizes shown in Fig. 2a correspond to the surface section of these channels. The large ones were in oval shape with dimension of 50–100 μm. Between them were some small honeycomb pores with less than 10-μm diameter. These suggest that the parallel tubes were different in interior diameter. Figure 2b corresponds to the cross section of the mini-chunk electrode. It is clear to observe the internal surfaces of the parallel channels with different diameters. The wall thickness between the channels is estimated to be 2 μm. These tubular channels in the biochar provide enough space for electrolyte solution to go through the biochar electrode and increase the electrolyte and electrode interfaces. Figure 2c shows the appearance of thin-film electrode. The film is flat without crack and the powders are packed loosely and randomly. In the magnified image of the thin-film electrode shown in Fig. 2d, the ground biochar particles sized between 10 and 40 μm, and maintain the microstructure of raw biochar materials with some small pores. But the tubular channels were shortened after the mini-chunk was ground into the powders.

Figure 3a shows the nitrogen adsorption isotherms of the activated maple biochar. The BET specific area is 303 m^2 g^{-1}, similar to that of the biochar studied previously [25]. The pore size distribution curve is shown in Fig. 3b. The peak pore size of this sample centered at 0.5–1.0 nm, which is located in micropore range. This class of micropores can be accessed by aqueous electrodes and contribute to electrochemical capacitance. The Raman spectroscopy result is shown in Fig. 4. The peak located around 1,345 and 1,570 cm^{-1} are attributed to the disorder-induced D band and graphite G band, respectively. The relative intensity between the D versus G band is associated with the increase of carbon disorder. The relative intensity is 0.98, suggesting that high ratio of ordered graphite carbon has been formed in the maple biochar.

Cyclic voltammograms measured at different scan rates for the supercapacitors with mini-chunk and thin-film electrodes are shown in Fig. 5. The CV curves of both electrodes show similar quasi-rectangular shape, indicating excellent ion transport behavior and similar electrochemical behavior. No obvious redox peaks were observed from the CV curves. This indicates that the supercapacitors are charged and discharged at a pseudo constant rate over the entire voltammetric cycles [26]. The CV curves became more rectangular at a lower scan rate and show increased distortion as the high scan rate is increased. That is mainly attributed to the limited diffusion and migration of electrolyte ions in the bulk, which is a common disadvantage of carbon monoliths [23]. From the CV curves, the capacitance can be estimated from the enclosed area of the cyclic voltammograms, the potential window, and the scan rate. The two electrodes have similar specific capacitance as they show nearly the same curves at the same scan rate, implying that the mini-chunk electrode has the similar CV properties of the thin-film electrode in biochar supercapacitors.

The charge–discharge behaviors of the two electrodes were characterized under galvanostatic conditions. At the same current density of 0.5 A g^{-1}, the curves of two electrodes show similar triangular shape, indicating the similar capacitive behavior. There is a sudden voltage drop

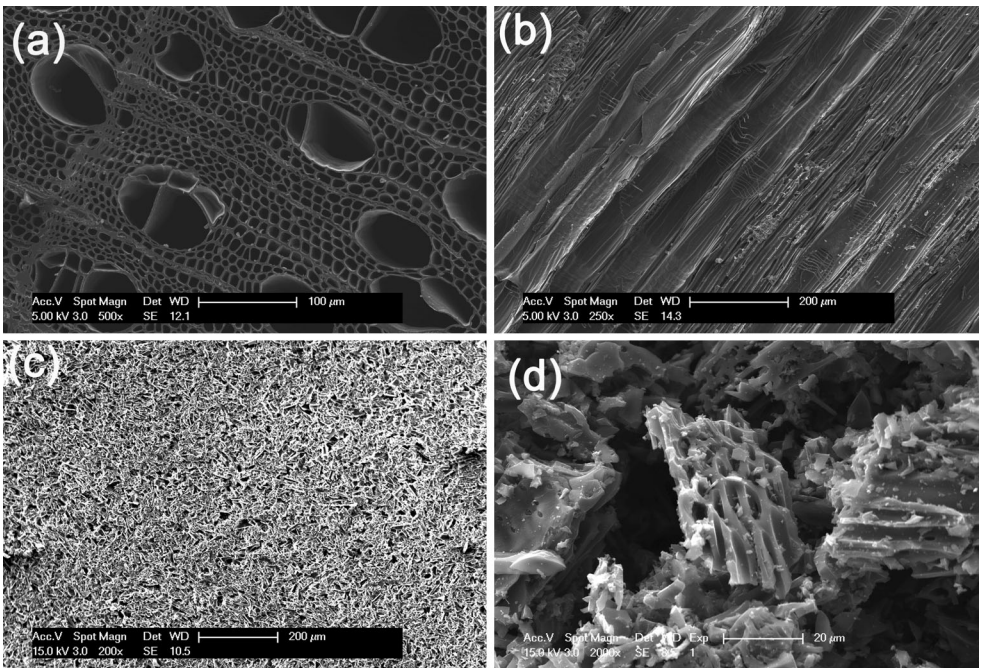

Fig. 2 SEM images of supercapacitors electrodes. **a** Surface section of a mini-chunk electrode; **b** cross section of a mini-chunk electrode; **c** surface section of a thin-film electrode; **d** magnification of the thin-film electrode

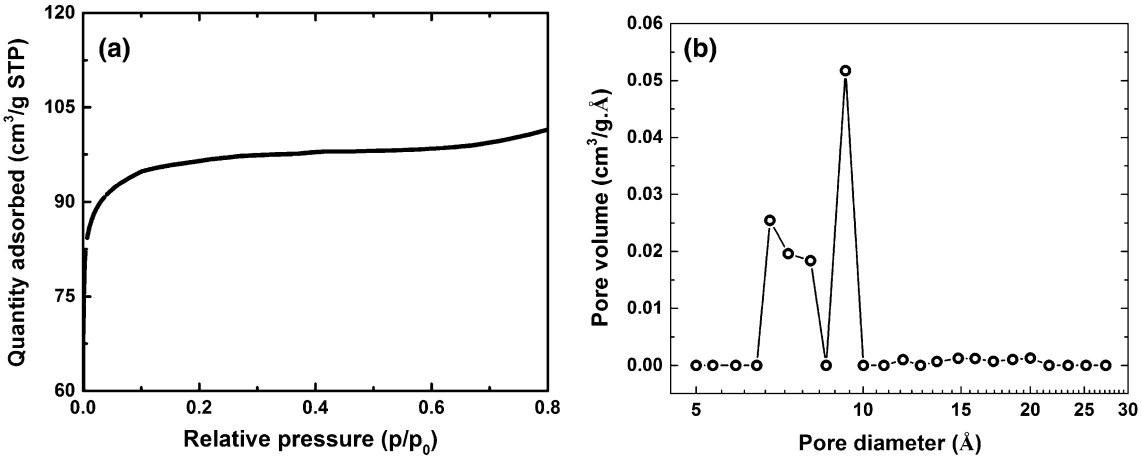

Fig. 3 Adsorption isotherm (**a**) and BJH adsorption plot (**b**) for maple biochar powder

in the charge and discharge voltage–time profiles, which is due to the ohmic drop (also known as IR) at the initial stage of the charge and discharge process. The specific capacitance C_m (in F g^{-1}) can be calculated from the galvanostatic charge–discharge curves according to the following equation:

$$C_m = \frac{C}{m} = \frac{I \times \Delta t}{\Delta V \times m}, \quad (1)$$

where I (A) is the discharge current, Δt (s) is the discharging time, ΔV (V) represents the potential drop during the discharge process, and m (g) is the mass of the biochar content in electrodes [23]. With the same current density (I/m), the slope of the linear part of the curves ($\Delta V/\Delta t$) determines the specific capacitance. So with similar slope of charge–discharge curves, these two electrodes show similar specific capacitors. The dependence of specific capacitance on the charge–discharge current density is listed in Fig. 6b. The mini-chunk and thin-film supercapacitors show the very close specific capacitance as the current densities were increased 0.5–2.0 A g^{-1}. When 0.5 A g^{-1} current was applied, the specific capacitance is 31 F g^{-1} for the mini-chunk supercapacitor and 32 F g^{-1} for the thin-film supercapacitor. As the supercapacitor

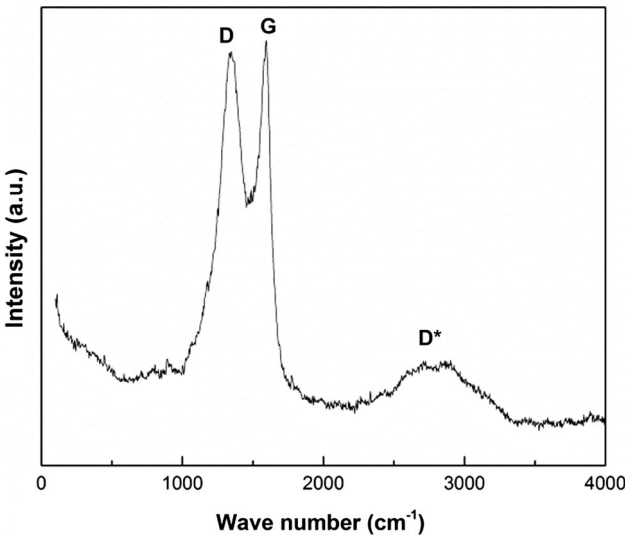

Fig. 4 Raman spectra of maple biochar sample

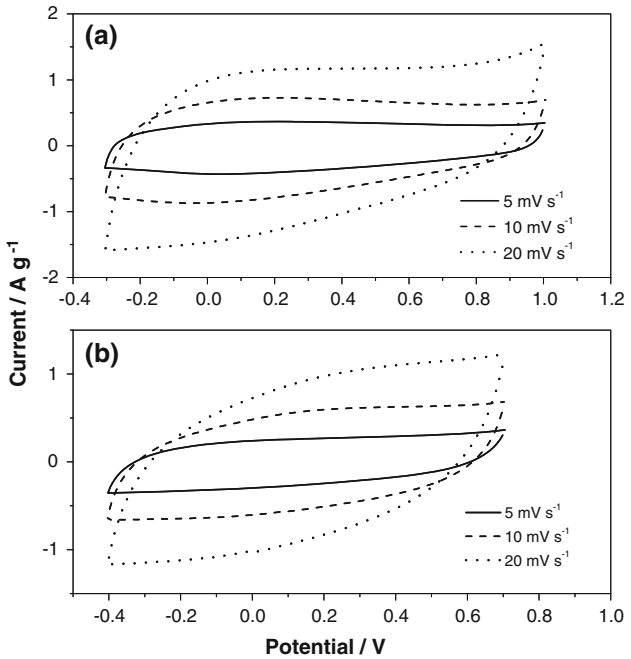

Fig. 5 Dependence of cyclic voltammograms for a biochar mini-chunk (**a**) or thin-film (**b**) supercapacitor as a function of scan rate

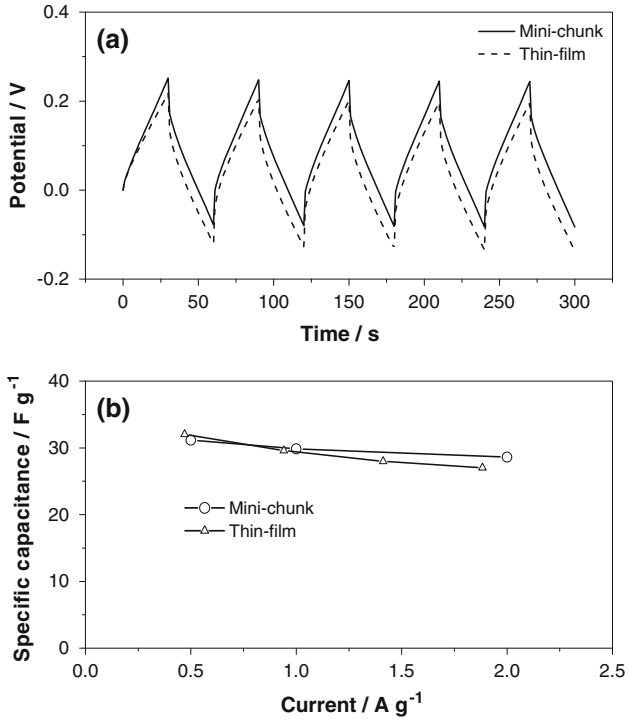

Fig. 6 **a** Potential-time transients for biochar mini-chunk (*solid*) or thin-film (*dash*) supercapacitor upon applying a 0.5 A g^{-1} polarization of 30 s for five cycles; and **b** their dependence of specific capacitance on charge–discharge current

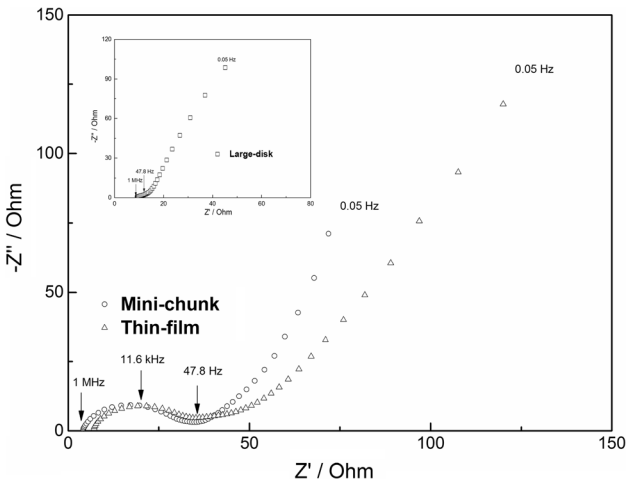

Fig. 7 Electrochemical impedance spectra for a biochar mini-chunk (**a**) or thin-film (**b**) supercapacitor measured at 600 mV. *Inset* The spectra for a large-disk-chunk capacitor

constructed with two symmetrical electrodes, the specific cell capacitance is only one fourth of that of an individual electrode. This result is favorably comparable to the supercapacitors employing advanced carbon materials such as graphene and carbon nanotube as the electrodes [27].

To further study the capacitive behavior of the biochar supercapacitors, the electrochemical impedance spectroscopies were measured from 100 M to 50 m Hz. The first intercept on the real-axis at high frequency corresponds to the ohmic resistances stemming from the electrolyte solution, the lead wire, the separator, and the contact between the electrode and the current collector [28]. The intercepts between low and high frequency correspond to electrode reaction resistance. In Fig. 7, the intercepts between low and high frequency of the impedance spectra of the mini-

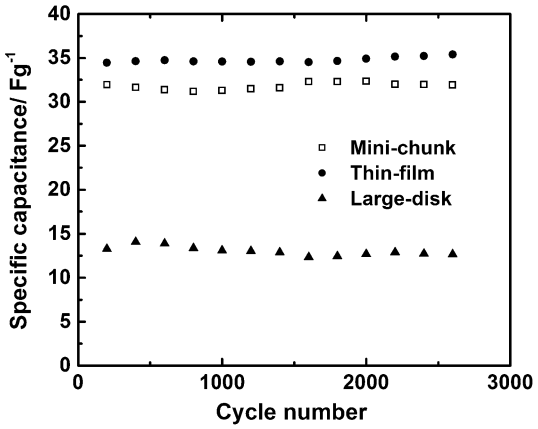

Fig. 8 Variation of specific capacitance as a function of cycle number for a biochar mini-chunk, thin-film, and large-disk-chunk supercapacitor

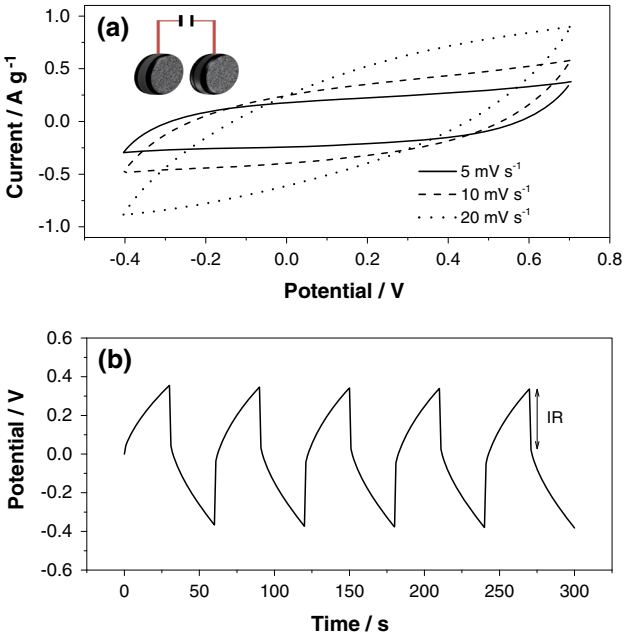

Fig. 9 CV curves recorded at various scan rates (**a**) and potential-time transients under a galvanostatic polarization at 0.5 A g^{-1} (**b**) for a biochar supercapacitor comprising of two large-disk-chunck electrodes in 0.5 mol L^{-3} H_2SO_4

chunk and thin-film supercapacitors are very close, suggesting the similar electrode reaction resistance of the mini-chunk electrode and thin-film electrode. In the low frequency region, the impedance plot generally shows an almost linear behavior. The steeper slope indicates that double-layer charge-storage phenomena are more dominant [28]. The deviation of the phase angle of the linear region from theoretical 90° is probably caused by the pore structure of biochar electrodes.

The stability of the biochar supercapacitors with mini-chunk and thin-film electrodes was evaluated using potential cycles. The specific capacitance calculated from CV curves as a function of the cycle number is plotted in Fig. 8. After 2,600 cycles, the mini-chunk and thin-film supercapacitors keep high capacitance without obvious degradation, indicating that both of them have good stability. Their specific capacitances are very close. The slightly lower value of the mini-chunk supercapacitor will be discussed in the following sections.

Based on the above CV curves, galvanostatic charge–discharge curves, AC impedance spectra, and the durability test, the mini-chunk electrodes demonstrates the same capacitive behavior of thin-film electrodes. Without using binder and complicated procedures for fabricating thin-film electrodes, the mini-chunk electrode provides a simple and fast method to characterize the supercapacitive performance of biochar materials. Moreover, the mini-chunk supercapacitor can be directly used as an mF-scale supercapacitor.

We have further evaluated the potential of developing an F-scale biochar supercapacitor using larger biochar chunk electrodes. The schematic diagram of a large-disk-chunk biochar supercapacitor is shown in an inset to Fig. 9a. The disk-chunk electrode used has a thickness of 700 μm, a geometric disk area of 0.18 cm^2, and a mass of 0.083 g. It is approximately 80 times heavier than the mini-chunk electrode used above. Figure 9a shows that the CV curves are still in a quasi-rectangular shape, but the enclosed area is much smaller compared to those for the mini-chunk and thin-film supercapacitors. In the galvanostatic charge–discharge curves shown in Fig. 9b, an immediate potential drop of 0.40 V was observed once 0.5 A g^{-1} current was applied. This high value strongly indicates that there is a high ohmic resistance associated with the large-disk-chunk electrode. In the impedance spectra shown in the inset to Fig. 7, the large-disk-chunk supercapacitor shows a non-linear region at low frequency. This deviation from the linear regions observed for the mini-chunk and thin-film supercapacitors indicates that the capacitive behavior for the large-disk-chunk supercapacitor is more complicated. The durability evaluation of the large-disk-chunk supercapacitor was shown in Fig. 8. Its performance is stable over 2,600 cycles but with lower specific capacitance (13 F g^{-1}).

Taken all together, the large-disk electrode exhibits much worse capacitive properties. In the charge–discharge voltage–time profiles shown in Fig. 9b, the sudden voltage drops correspond to the ohmic drop (IR) at the initial stage of the charge and discharge processes. The large-disk electrode exhibited a larger IR drop of 0.40 V while the IR drop for mini-chunk electrode and film electrode was only 0.08 V. The reasons are two folds. Firstly, the longer tubular channels in the large-disk electrode cause a higher

ohmic resistance for the electrolyte penetration. Secondly, there is need to improve the electrical contact between the large-disk-chunk electrode and the current collector. In the contrast, the tubular channel is much shorter in the mini-chunk electrode, and partially broken in the thin-film electrodes, which accounts for a relatively higher specific capacitance of thin-film electrode than that of mini-chunk electrodes (Fig. 8). Therefore, there is a need to optimize large-disk-chunk electrodes for F-scale supercapacitor applications because of high resistance response.

4 Conclusions

Three types of biochar supercapacitor electrode, mini-chunk electrodes, thin-film electrodes, and large-disk-chunk electrodes were studied for supercapacitor applications. Both the mini-chunk and thin-film electrodes showed good capacitive performance of approximately 30 F g^{-1} in two symmetrical electrode supercapacitors and no degradation after 2,600 CV cycles. However, the large-disk electrodes exhibited worse capacitive properties because of the large resistance caused by the long tubular channels. The capacitive performance of thin-film electrodes can be reproduced in the small monolith of mini-chunk electrode. Without using binder and other additives, the mini-chunk electrode technique provides a simple and fast technique to evaluate various biochar materials for supercapacitor applications. The mini-chunk biochar supercapacitor can be directly used an mF-scale supercapacitor power source.

Acknowledgments We gratefully acknowledge the financial support from Illinois Hazardous Waste Research Fund, and the Hetero-FoaM Center, an Energy Frontier Research Center funded by the U.S. Department of Energy, Office of Science, Basic Energy Sciences under Award #DESC0001061.

References

1. Xiong G, Meng C, Reifenberger RG, Irazoqui PP, Fisher TS (2014) A review of graphene-based electrochemical microsupercapacitors. Electroanal 26:30–51
2. Adhyapak P, Maddanimath T, Pethkar S, Chandwadkar A, Negi Y, Vijayamohanan K (2002) Application of electrochemically prepared carbon nanofibers in supercapacitors. J Power Sources 109:105–110
3. Mayer S, Pekala R, Kaschmitter J (1993) The aerocapacitor: an electrochemical double-layer energy-storage device. J Electrochem Soc 140:446–451
4. Yoshida A, Nonaka S, Aoki I, Nishino A (1996) Electric double-layer capacitors with sheet-type polarizable electrodes and application of the capacitors. J Power Sources 60:213–218
5. Simon P, Gogotsi Y (2008) Materials for electrochemical capacitors. Nat mater 7:845–854
6. Beidaghi M, Gogotsi Y (2014) Capacitive energy storage in micro-scale devices: recent advances in design and fabrication of micro-supercapacitors. Energy Env Sci 7:867–884
7. Wang H, Casalongue HS, Liang Y, Dai H (2010) $Ni(OH)_2$ nanoplates grown on graphene as advanced electrochemical pseudocapacitor materials. J Am Chem Soc 132:7472–7477
8. Xu X, Liang J, Zhou H, Ding S, Yu D (2014) The preparation of hierarchical tubular structures comprised of NiO nanosheets with enhanced supercapacitive performance. RSC Adv 4:3181–3187
9. Xu X, Zhou H, Ding S, Li J, Li B, Yu D (2014) The facile synthesis of hierarchical NiCoO2 nanotubes comprised ultrathin nanosheets for supercapacitors. J Power Sources 267:641–647
10. Wang YG, Li HQ, Xia YY (2006) Ordered whisker-like polyaniline grown on the surface of mesoporous carbon and its electrochemical capacitance performance. Adv Mater 18:2619–2623
11. Frackowiak E (2007) Carbon materials for supercapacitor application. Phys Chem Chem Phys 9:1774–1785
12. Portet C, Taberna PL, Simon P, Flahaut E, Laberty-Robert C (2005) High power density electrodes for carbon supercapacitor applications. Electrochim Acta 50:4174–4181
13. Qu D, Shi H (1998) Studies of activated carbons used in double-layer capacitors. J Power Sources 74:99–107
14. Yan X, Tai Z, Chen J, Xue Q (2011) Fabrication of carbon nanofiber–polyaniline composite flexible paper for supercapacitor. Nanoscale 3:212–216
15. Gómez-Romero P, Chojak M, Cuentas-Gallegos K, Asensio JA, Kulesza PJ, Casañ-Pastor N, Lira-Cantú M (2003) Hybrid organic–inorganic nanocomposite materials for application in solid state electrochemical supercapacitors. Electrochem Commun 5:149–153
16. Mdoe J, Mkayula L (2002) Preparation and characterization of activated carbons from rice husks and shells of palm fruits. Tanzan J Sci 28:131–142
17. Chen M, Kang X, Wumaier T, Dou J, Gao B, Han Y, Xu G, Liu Z, Zhang L (2013) Preparation of activated carbon from cotton stalk and its application in supercapacitor. J Solid State Electrochem 17:1005–1012
18. Laird DA, Brown RC, Amonette JE, Lehmann J (2009) Review of the pyrolysis platform for coproducing bio-oil and biochar. Biofuels Bioprod Biorefin 3:547–562
19. Dobele G, Dizhbite T, Gil M, Volperts A, Centeno T (2012) Production of nanoporous carbons from wood processing wastes and their use in supercapacitors and CO_2 capture. Biomass Bioenergy 46:145–154
20. Azargohar R, Dalai A (2006) Biochar as a precursor of activated carbon. In: Twenty-seventh symposium on biotechnology for fuels and chemicals. Springer, Berlin, pp 762–773
21. Kitano M, Arai K, Kodama A, Kousaka T, Nakajima K, Hayashi S, Hara M (2009) Preparation of a sulfonated porous carbon catalyst with high specific surface area. Catal Lett 131:242–249
22. Teng H, Yeh TS, Hsu LY (1998) Preparation of activated carbon from bituminous coal with phosphoric acid activation. Carbon 36:1387–1395
23. Liu MC, Kong LB, Zhang P, Luo YC, Kang L (2012) Porous wood carbon monolith for high-performance supercapacitors. Electrochim Acta 60:443–448
24. Jin H, Wang X, Gu Z, Polin J (2013) Carbon materials from high ash biochar for supercapacitor and improvement of capacitance with HNO_3 surface oxidation. J Power Sources 236:285–292
25. Jiang J, Zhang L, Wang X, Holm N, Rajagopalan K, Chen F, Ma S (2013) Highly ordered macroporous woody biochar with ultra-high carbon content as supercapacitor electrodes. Electrochim Acta 113:481–489
26. Lang X, Hirata A, Fujita T, Chen M (2011) Nanoporous metal/oxide hybrid electrodes for electrochemical supercapacitors. Nat Nanotechnol 6:232–236
27. Frackowiak E, Beguin F (2001) Carbon materials for the electrochemical storage of energy in capacitors. Carbon 39:937–950
28. Ghosh A, Lee YH (2012) Carbon-based electrochemical capacitors. ChemSusChem 5:480–499